Numerical simulation of nasal resistance using three-dimensional models of the nasal cavity and paranasal sinus

Shoji Kaneda[1], Fumiyuki Goto[2], Kenji Okami[3], Reo Mitsutani[4], and Yoko Takakura[4]

[1]Tokai University School of Medicine
[2]Tokai University School of Medicine Graduate School of Medicine
[3]Tokai University - Isehara Campus
[4]Tokai University

February 22, 2024

Abstract

Objectives: Previously, we used a nasal cavity model to analyze the intranasal airflow dynamics and numerically calculate the nasal resistance value. Here, we created a nasal sinus model that is closer to the real human body and calculated the nasal resistance value. Moreover, we performed comparisons of the measured and simulation data. Setting: The models were healthy adult volunteers: a 35-year-old man (model 1) and a 25-year-old man (model 2), who were used as nasal cavity and paranasal sinus models. A 1.0-mm slice computed tomography (CT) was performed and a nasal sinus model was created. We compared the nasal resistance of the simulation value with that of the measured value obtained using rhinomanometry. Results: In model 1, the measured (simulation) value was 0.69 (0.48) on the right, 1.10 (0.41) on the left, and 0.42 (0.22) on both sides. In model 2, the measured (simulation) value was 0.72 (0.21) on the right, 0.32 (0.09) on the left, and 0.22 (0.06) on both sides. Conclusion: We observed a difference between the simulation and measured values, possibly because of the length of the inferior turbinate and the cross-sectional area of the choana and nasopharynx. Further experiments using additional nasal cavity and paranasal sinus models are warranted.

Numerical simulation of nasal resistance using three-dimensional models of the nasal cavity and paranasal sinus

Abstract

Objectives: Previously, we used a nasal cavity model to analyze the intranasal airflow dynamics and numerically calculate the nasal resistance value. Here, we created a nasal sinus model that is closer to the real human body and calculated the nasal resistance value. Moreover, we performed comparisons of the measured and simulation data.

Setting: The models were healthy adult volunteers: a 35-year-old man (model 1) and a 25-year-old man (model 2), who were used as nasal cavity and paranasal sinus models. A 1.0-mm slice computed tomography (CT) was performed and a nasal sinus model was created. We compared the nasal resistance of the simulation value with that of the measured value obtained using rhinomanometry.

Results: In model 1, the measured (simulation) value was 0.69 (0.48) on the right, 1.10 (0.41) on the left, and 0.42 (0.22) on both sides. In model 2, the measured (simulation) value was 0.72 (0.21) on the right, 0.32 (0.09) on the left, and 0.22 (0.06) on both sides.

Conclusion: We observed a difference between the simulation and measured values, possibly because of the length of the inferior turbinate and the cross-sectional area of the choana and nasopharynx. Further experiments using additional nasal cavity and paranasal sinus models are warranted.

Keywords:

Nasal cavity and paranasal sinus model, Turbinates, Rhinomanometry, Computed tomography, Computational fluid dynamics

Key points

1. Computational fluid dynamics is the popular method for evaluating airflow.
2. Rhinomanometry is popular way for measurement of nasal resistance.
3. Nasal cavity and paranasal sinus have so complicated construction.
4. We created accurate nasal cavity and paranasal sinus 3D models and evaluated measured and simulation values of nasal resistance.
5. The length of the inferior turbinate and cross-sectional area of the choana and nasopharynx may affect the nasal resistance.

Introduction

Many patients have nasal obstruction in rhinology disease. For the evaluation of nasal obstruction, rhinomanometry is very popular worldwide.[1] Rhinomanometry can measure nasal pressure and airflow during inspiration and expiration. Additionally, it can measure nasal resistance to measure the pressure difference between the nostril and choana. Nasal resistance can be affected by alternating congestion and decongestion of the nasal mucosa, which is termed the nasal cycle.[2, 3] Lang et al. investigated the nasal cycle using endoscopy, rhinoresistometry, and acoustic rhinometry.[4] Gogniashvili et al. also investigated the nasal cycle in the same manner.[5] In general anesthesia, nasal patency is investigated before nasal intubation.[6] Rhinomanometry can measure nasal resistance during the nasal cycle; however, it cannot measure the direct airflow pressure in the nasal cavity.

Recently, computational fluid dynamics (CFD) in rhinology has been popular for measuring airflow or pressure.[7, 8] This enables the observation of the airflow, pressure, heat, and streamline, which cannot be determined directly. Kim et al. reviewed patient-specific CFD models of nasal airflow.[9]Moreover, Wang et al. simulated applying CFD to the study of the nasal cavity in 2005.[10] In turn, Xiong et al. reported a numerical flow simulation in virtual post-endoscopic sinus surgery.[11] Twenty-two healthy adults were studied to determine the normal nasal airflow.[12] It was found that nasal resistance affected nasal obstruction. Recently, these phenomena were simulated using CFD. Radulesco reported a comparison of nasal obstruction with CFD variables.[13] Finally, Berger reported the agreement between rhinomanometry and CFD regarding nasal resistance.[14]

CFD can be achieved by creating a 3D model and using numerical simulation. However, the nose is composed of the nasal cavity and paranasal sinus and is a very complicated structure. Thus, it is very difficult to create a highly accurate nasal cavity and paranasal sinus 3D model. The recent literature includes many CFD rhinology documents, with absence of accurate nose 3D models. Therefore, we created a nose 3D model to check the all-natural ostium of all paranasal sinuses. It was unclear whether the simulation in reality reflected the human body. By comparing the real nasal resistance value, which can be measured, with the numerical simulation value, it is possible to judge whether or not it is closer to the human body.

Objective

In this research, we compared the measured and calculated nasal resistance values using the newly created nasal cavity and paranasal sinus model. We streamlined these data and studied the relationship between the model and nasal resistance.

Method

The sample size was two. The models included a 35-year-old male (model 1) and a 25-year-old male (model 2) who participated in the study as healthy adult volunteers. Sections with a width of 1.0 mm and a pixel size of $0.488 \times 0.488 \times 0.488$ mm were collected and scanned using a CT instrument (SIEMENS SOMATOM Definition Edge®, Germany), and a nasal cavity and paranasal sinus 3D model was created using Mimics

23.0® (Materialize, Belgium) (Fig. 1). We checked all CT slices and natural ostium and remodeled them. Therefore, we prepared two accurate nasal cavity and paranasal sinus 3D models.

Moreover, 3-matic 15.0® (Materialize, Belgium) was used for mesh formation after the smoothing procedure. The TetGen mesh generator was used here with the boundary condition that the boundary surface must remain intact (unchanged), both at the vertices and the triangles. This means that if tetrahedron vertices (called Steiner points in Delauney terminology) are to be added by the algorithm, they are never added at the boundary surface, but only at the interior of the model. The number of surface meshes was 177448 in Model 1 and 136332 in Model 2. The number of volume meshes was 353933 in Model 1 and 285874 in Model 2. The number of nodes was 103629 in Model 1 and 82312 in Model 2. The grid convergence of these models was calculated. We confirmed that the number of volume meshes of these models were appropriate.

Fluent 17.2® (ANSYS, American) was employed for fluid analysis using the continuity equation for three-dimensional incompressible flow and the Navies–Stokes equation for the basic equations. Both models were Laminar models. The SIMPLE calculation method using the finite volume method was employed here, and the quadratic precision upwind difference method was used to discretize the convection terms.

The boundary condition was as follows:

i) the velocity is equal to zero at the nasal wall;

ii) a pressure of zero is presumed at the nostrils as the atmospheric pressure;

iii) at the trachea side, the velocity (v) is given.

In the steady solution, the iteration number was 300. In turn, in the unsteady solution, the iteration number was 20/time step and the time step width was 0.001 [s]. We used a sine function of 3 s per period as the breath airflow.

The nasal resistance value, R [Pa/(cm^3/s)], was calculated by the following formula using the flow rate V [cm^3/s] at the nostril when the pressure difference (ΔP) between the atmospheric pressure and the pharynx was 100 [Pa]:

R = [?]P/V,

where R is the nasal resistance [Pa/(cm^3/s)], ΔP is the differential pressure between the atmospheric pressure and the pharynx [Pa], and V is the flow rate [cm^3/s].

After the calculation of the resistance for each cavity, the right resistance (R_{right}) and left resistance (R_{left}) were calculated, with the total resistance for both cavities, R_{total}, being calculated as follows:

$1/R_{total} = 1/R_{right} + 1/R_{left}$.

First, we performed a simulation at the flow velocity of 1.5 (m/s) applied to the pharyngeal side in the steady solution. A pressure difference of Δ100 [Pa] is required to measure the nasal resistance value. Second, we performed a simulation in the same condition in the unsteady solution for the nasal resistance. The maximum flow velocity in Model 1 was 1.5 (m/s) on the right and 1.5 (m/s) on the left. Moreover, in Model 2, the maximum flow velocity was 3.0 (m/s) on the right and 6.0 (m/s) on the left in the unsteady solution.

Rhinometry was performed using an MPR-3100® instrument (Nihonkoden, Japanese). Nasal resistance was measured in the two subjects using active anterior rhinometry (without vasoconstriction). To rule out the effect of the nasal cycle, nasal resistance was measured right after CT.

Ethical Consideration

All procedures used in this research were approved by the Ethical Committee of XXXX (approval number: XXXX).

Reporting guidelines

STROBE checklist (for observational studies) was followed for this study.

Results

The simulation values were obtained in the unsteady solution. The nasal resistance measured (simulation) values of Model 1 were 0.69 (0.48) on the right, 1.10 (0.41) on the left, and 0.42 (0.22) on both sides. The actual measurement (simulation) values of Model 2 were 0.72 (0.21) on the right, 0.32 (0.09) on the left, and 0.22 (0.06) on both sides (Fig. 2).

Additionally, the velocity vector of Models 1 and 2, as assessed using a steady-state calculation, is shown in Figure 3. The speed near the choana was suddenly reduced in Model 1. Conversely, the speed remained unchanged in Model 2.

The streamlining of Models 1 and 2 using a steady-state calculation is shown in Figures 4 and 5. In Model 1, we observed ventilation in the right maxillary sinus and in both ethmoidal sinuses. Conversely, we did not observe ventilation in the left maxillary sinuses or in both frontal sinuses (Fig. 4). Additionally, in Model 2, we did not observe ventilation in frontal and maxillary sinuses (Fig.5).

Discussion

Two accurate nasal cavity and paranasal sinus models were created, and numerical simulation of nasal ventilation was performed. In our research, in the simulation that was performed using the nasal cavity model without the sinuses, the magnitude of the relationship was correct, but the simulation value tended to be lower than the actual measurement, although a similar tendency was observed.[15] By including the paranasal sinuses, the simulation was expected to approach the measured value because it would be closer to the actual shape; however, this was not the case. This discrepancy can be attributed to the fact that the airflow in the model shown in Figure 4 hardly entered the paranasal sinuses.

There are two possible explanations for the observation that Model 1 had a higher nasal resistance value than did model 2. 1) In Model 1, the cross-sectional area became smaller than that of Model 2 as it approached the choana; thus, the flow velocity increased from the continuity equation. As the flow velocity increased, the pressure decreased based on Bernoulli's principle.

2) The difference in the cross-sectional areas of the nasopharynx compared with the choana was larger in Model 1 than in Model 2. Thus, an energy loss occurred because of the reverse pressure gradient according to the rapid expansion of the cross-sectional area; it became a pressure loss, and the pressure drop became even larger (Fig. 6).

Ventilation into the sinuses remains uncertain, but it is unlikely that there is no ventilation. In our study, Model 1 exhibited ventilation in the maxillary and ethmoidal sinuses exclusively. Kumar et al. reported the air flow in the periods pre- and post-endoscopic sinus surgery using numerical simulation.[16] However, the 3D model reported by them in pre-surgery did not connect the nasal cavity with the frontal sinus and maxillary sinus. Therefore, it was too difficult to create an accurate 3D model. The natural ostium connecting the sinuses and the nasal cavity may not be accurately created. To date, it has been reported that the nasal sinus model is used to examine the correlation between the nasal air permeability measurement and the numerical simulation, and, although they are similar, they do not completely match.[14] Radulesco et al. reported the measured and simulated nasal resistance before septoplasty using 22 nasal cavity models. The perceptions of the patients and the measured and simulation nasal resistance exhibited strong correlations. However, the measured and simulation nasal resistance were poorly correlated.[17] Tretiakow et al. investigated the workflow for creating a 3D model for accurate CFD.[18]We think that it is necessary to create an accurate nasal sinus model for more accurate simulation.

Our results suggest that the length of the inferior turbinate and the cross-sectional area of the nasopharynx and the choana affect the nasal resistance value. Hariri et al. reported that inferior turbinate weight loss reduced nasal resistance in 3 of 5 models, whereas it remained unchanged in the remaining two models. In the two cases without change, the nasal resistance was affected by factors other than the inferior turbinate.[19]

The relationship between the length of the inferior turbinate and the cross-sectional area encompassing the nasopharynx, as in this example, may also affect the nasal resistance value. However, the sample size used in our investigation was 2 volunteers, which was too small to conclude on the effect of nasal resistance in this context. A larger sample size is needed for further investigation.

Conclusions

In conclusion, using the two nasal cavity and paranasal sinus models, the nasal resistance value was calculated via numerical simulation. The length of the inferior turbinate and cross-sectional area of the choana and nasopharynx may affect the nasal resistance. A more accurate model is needed for future simulations.

References

1. Scadding G, Hellings P, Alobid I, et al. Diagnostic tools in Rhinology EAACI position paper. Clin Transl Allergy. 2011 Jun 10;1(1):2.
2. Hasegawa M, Kern EB. Variations in nasal resistance in man: a rhinomanometric study of the nasal cycle in 50 human subjects. Rhinology. 1978 Mar 1;16(1):19–29.
3. Eccles R. Nasal airflow in health and disease. Acta Oto-Laryngol. 2000 Jan 1;120(5):580–95.
4. Lang C, Grutzenmacher S, Mlynski B, et al. Investigating the nasal cycle using endoscopy, rhinoresistometry, and acoustic rhinometry. Laryngoscope. 2003 Feb;113(2):284–9.
5. Gogniashvili G, Sh J, Khujadze M. Investigation of the nasal cycle function through endoscopy, rhinoresistometry, and acoustic rhinometry. Georgian News. 2009 Sep 1;174:22–25.
6. Shohara K, Goto T, Kuwahara G, et al. Validity of rhinometry in measuring nasal patency for nasotracheal intubtion. J Anesth. 2016 Oct 13;31(1):1–4.
7. Wong E, Inthavong K, Singh N. Comment on the European position paper on diagnostic tools in rhinology â\euro" computational fluid dynamics. Rhinology. 2019 Dec 1;57(6):477–8.
8. Quadrio M, Pipolo C, Corti S, et al. Review of computational fluid dynamics in the assessment of nasal air flow and analysis of its limitations. Eur Arch Otorhinolaryngol. 2014 Sep;271(9):2349–54.
9. Kim SK, Na Y, Kim JI, Chung SK. Patient specific CFD models of nasal airflow: overview of methods and challenges. J Biomech. 2013 Jan 18;46(2):299–306.
10. Wang K, Denney TS, Morrison EE, Vodyanov VJ. Numerical simulation of air flow in the human nasal cavity. 2005 IEEE Engineering in Medicine and Biology 27th Annual Conference. 2006 Jan 17:5607–10.
11. Xiong G, Zhan J, Zuo K. et al. Numerical flow simulation in the post-endoscopic sinus surgery nasal cavity. Med Biol Eng Comput. 2008 Aug 26;46(11):1161–7.
12. Zhao K, Jiang J. What is normal nasal airflow? A computational study of 22 healthy adults. Int Forum Allergy Rhinol 2014 Mar 24;4(6):435–46.
13. Radulesco T, Meister L, Bouchet G, et al. Functional relevance of computational fluid dynamics in the field of nasal obstruction: a literature review. Clin Otolaryngol. 2019 Jun 24;44(5):801–9.
14. Berger M, Giotakis AI, Pillei M, et al. Agreement between rhinomanometry and computed tomography-based computational fluid dynamics. Int J Comput Assist Radiol Surg. 2021 Mar 7;16(4):629–38.
15. Kaneda S, Iida M, Yamamoto H, et al. Evaluation of nasal airflow and resistance: computational modeling for experimental measurements. Tokai J Exp Clin Med. 2019 Sep 20;44(3):59–67.
16. Kumar H, Jain R, Douglas RG, Tawhai MH. Airflow in the human nasal passage and sinuses of chronic rhinosinusitis subjects. PLOS ONE. 2016 Jun 1;11(6):e0156379.
17. Radulesco T, Meister L. Bouchet G, et al. Correlations between computational fluid dynamics and clinical evaluation of nasal airway obstruction due to septal deviation: an observational study. Clin Otolaryngol. 2019 Apr 20;44(4):603–11.
18. Tretialow D, Tesch K. Three-dimensional modeling and automatic analysis of the human nasal cavity and paranasal sinuses using the computational fluid dynamics method. Eur Arch Oto-Rhino-L. 2020 Oct 17;278(5):1443–53.
19. Hariri BM, Rhee JS, Garcia GJ. Identifying patients who may benefit from inferior turbinate reduction using computer simulations. Laryngoscope. 2015 May 11;125(12):2635-41.

Figure Legends

Fig. 1 Findings from Models 1 and 2

Fig. 2 The results of nasal resistance in Models 1 and 2 in the numerical simulation and the comparison of nasal resistance between the simulation and measurement situations (the value of inspiration Δ100 Pa of nasal resistance R [Pa/cm^3/s])

Fig. 3 Velocity vector of Models 1 and 2

(a) Velocity vector of Model 1. The speed suddenly decreased near the choana ().

(b) Velocity vector of Model 2. The speed remained unchanged compared with model 1 ().

Fig. 4 Streamlining of Model 1; view from the front

(a) Right open streamline. Ventilation in the maxillary sinus and ethmoidal sinus; however, ventilation in the frontal sinus was not observed.

(b) Left open streamline. Ventilation of the frontal sinus and maxillary sinus was not observed.

Fig. 5 Streamlining of Model 2; view from the front

(a) Right open streamline. Ventilation of the frontal sinus and maxillary sinus was not observed.

(b) Left open streamline. Ventilation of the frontal sinus and maxillary sinus was not observed.

Fig. 6 Area of the posterior end of the inferior turbinate and nasopharyngeal section of Models 1 and 2

A comparison of the cross-sectional areas showed that the cross-sectional areas of Model 1 have changed significantly.

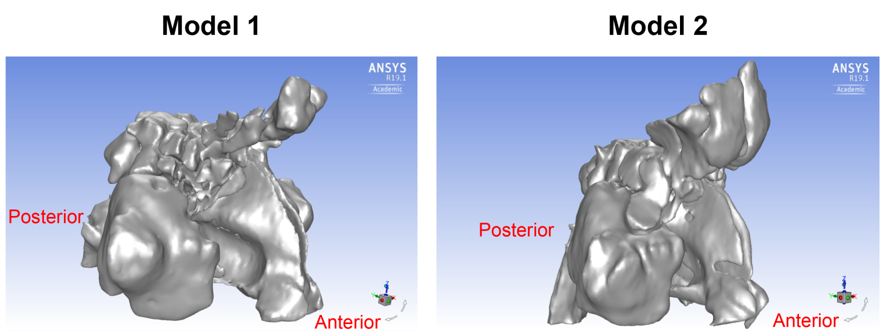

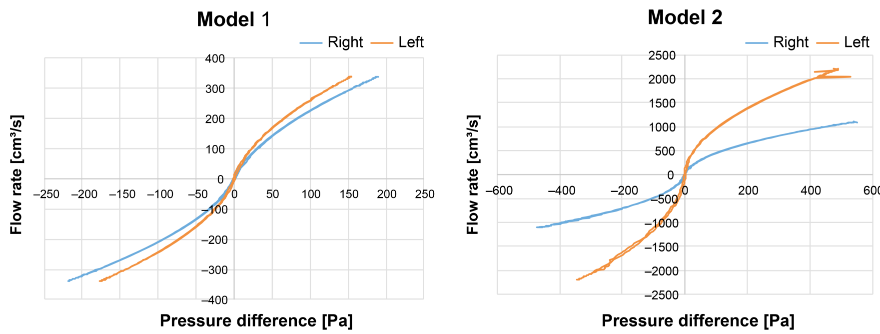

		Simulation	Measurement
Model 1	Right	0.48	0.69
	Left	0.41	1.10
	Both	0.22	0.42
Model 2	Right	0.21	0.72
	Left	0.09	0.32
	Both	0.06	0.22

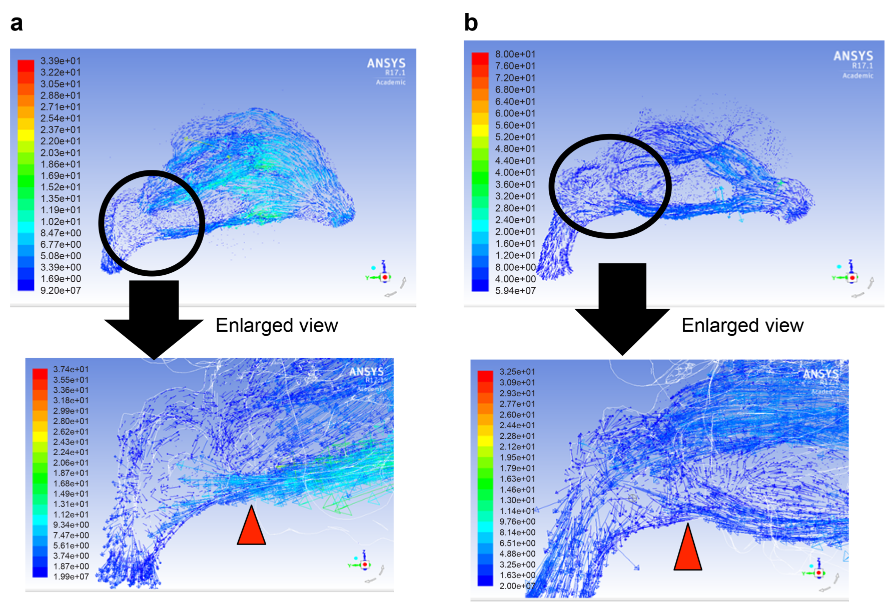

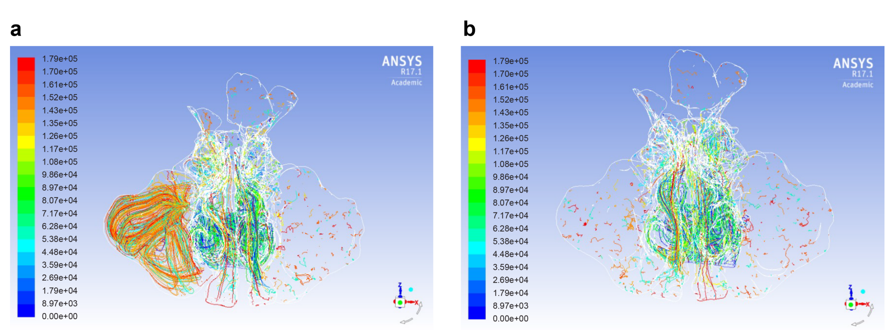

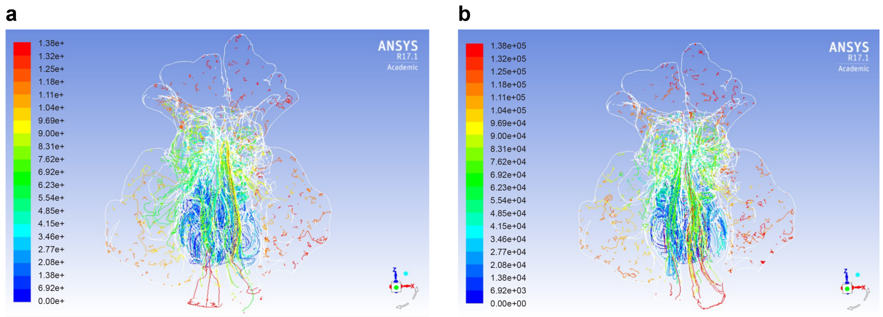
a
b
ANSYS
R17.1
Academic
1.38e+05
1.32e+05
1.25e+05
1.18e+05
1.11e+05
1.04e+05
9.69e+04
9.00e+04
8.31e+04
7.62e+04
6.92e+04
6.23e+04
5.54e+04
4.85e+04
4.15e+04
3.46e+04
2.77e+04
2.08e+04
1.38e+04
6.92e+03
0.00e+00

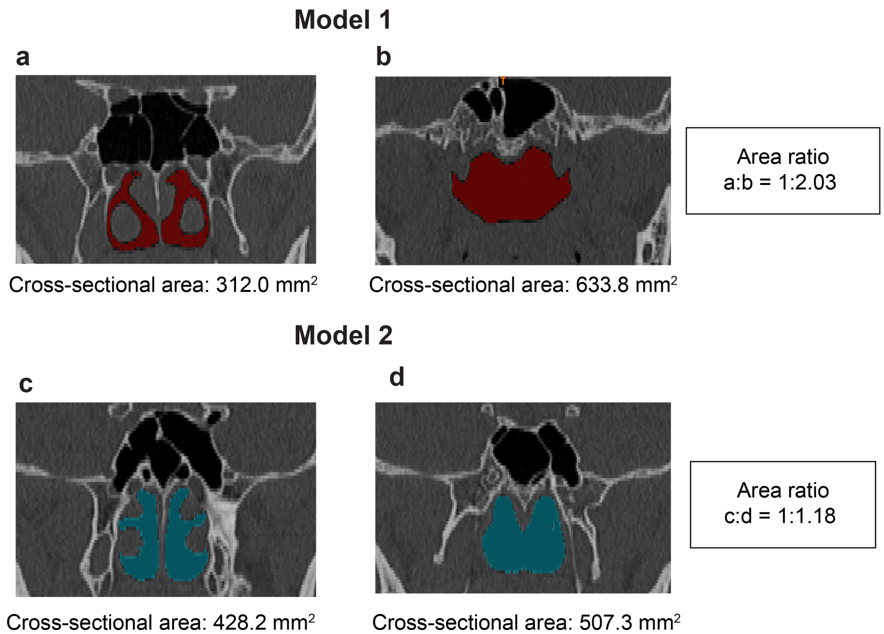
Model 1
a
b
Area ratio
a:b = 1:2.03
Cross-sectional area: 312.0 mm²
Cross-sectional area: 633.8 mm²
Model 2
c
d
Area ratio
c:d = 1:1.18
Cross-sectional area: 428.2 mm²
Cross-sectional area: 507.3 mm²